Eur. Phys. J. B **54**, 509–524 (2006)
DOI: 10.1140/epjb/e2007-00025-7

THE EUROPEAN PHYSICAL JOURNAL B

Bicontinuous geometries and molecular self-assembly: comparison of local curvature and global packing variations in genus-three cubic, tetragonal and rhombohedral surfaces

G.E. Schröder-Turk[a], A. Fogden, and S.T. Hyde

Dept. of Applied Maths, Research School of Physical Sciences, Australian National University, Canberra 0200 ACT, Australia

Received 5 June 2006 / Received in final form 11 October 2006
Published online 3 February 2007 – © EDP Sciences, Società Italiana di Fisica, Springer-Verlag 2007

Abstract. Balanced infinite periodic minimal surface families that contain the cubic Gyroid (G), Diamond (D) and Primitive (P) surfaces are studied in terms of their global packing and local curvature properties. These properties are central to understanding the formation of mesophases in amphiphile and copolymer molecular systems. The surfaces investigated are the tetragonal, rhombohedral and hexagonal tD, tP, tG, rG, rPD and H surfaces. These non-cubic minimal surfaces furnish topology-preserving transformation pathways between the three cubic surfaces. We introduce 'packing (or global) homogeneity', defined as the standard deviation Δd of the distribution of the channel diameter throughout the labyrinth, where the channel diameter d is determined from the medial surface skeleton centered within the labyrinthine domains. Curvature homogeneity is defined similarly as the standard deviation ΔK of the distribution of Gaussian curvature. All data are presented for distinct length normalisations: constant surface-to-volume ratio, constant average Gaussian curvature and constant average channel diameter. We provide first and second moments of the distribution of channel diameter for all members of these surfaces complementing curvature data from [A. Fogden, S. Hyde, Eur. Phys. J. B **7**, 91 (1999)]. The cubic G and D surfaces are deep local minima of Δd along the surface families (with G more homogeneous than D), whereas the cubic P surface is an inflection point of Δd with adjacent, more homogeneous surface members. Both curvature and packing homogeneity favour the tetragonal route between G and D (via tG and tD surfaces) in preference to the rhombohedral route (via rG and rPD).

PACS. 02.40.-k Geometry, differential geometry, and topology – 61.30.St Lyotropic phases – 81.16.Dn Self-assembly – 82.35.Jk Copolymers, phase transitions, structure

1 Introduction

The issue of transformations between hyperbolic surfaces is one of continuing relevance to our understanding of mesostructure and phase transformations in mesostructured matter. The presence of structures based on infinite periodic minimal surfaces (IPMS) of cubic symmetry is certain in bicontinuous cubic mesophases; the possible occurrence of non-cubic relatives as stable mesophases remains speculative, though their existence and similarities to their cubic counterparts suggest their relevance to physical systems. Observation and discussion of (pressure-induced) phase transitions between different cubic bicontinuous lyotropic phases in amphiphilic self-assemblies are increasingly common [1–5]. A related, more fundamental, issue also deserves detailed analysis. Despite the widespread occurrence of (particularly G and D) cubic periodic minimal surfaces in soft material assemblies, from amphiphilic liquid crystals to synthetic block copolymer materials and lipid-protein assemblies cell organelles in vivo, the reason why the majority of liquid-crystalline self-assemblies adopt cubic symmetry remains uncertain. We note recent reports of the cubic Gyroid phase in simulations of purely entropy-driven assemblies of hard pear-shaped particles [6], and reports of supramolecular assemblies that form crystalline, *anisotropic* (non-cubic) equilibrium phases, such as ABC block tripolymers [7–9]. A deeper understanding of relative stabilities of bicontinuous forms — including anisotropic examples — is needed. The issue is best addressed by studying surface families that are in general *not* cubic, but include singular members with cubic symmetry.

In this paper we analyse one-parameter families of IPMS with isolated members that are congruent to the cubic Primitive (P), Diamond (D) and Gyroid (G) surfaces. These surfaces, the tG, rG, rPD, tP, tD, H

[a] *Present address*: Institut für Theoretische Physik I, Friedrich-Alexander Universität Erlangen-Nürnberg, Staudtstr. 7, 91058 Erlangen, Germany
e-mail: Gerd.Schroeder-Turk@physik.uni-erlangen.de

discussed in [10], afford continuous pathways of intermediate structures that are embedded (intersection-free) minimal surfaces between the cubic cases.

We focus here on global properties of these surfaces, beyond surface-to-volume ratios, and compare those data with local curvature properties (The latter have already been studied extensively [10]). In particular, we analyse the structures in terms of *global (or packing) homogeneity* which provides a measure of the fluctuations of the pointwise channel diameter. Those global fluctuations are independent of local fluctuations of the Gaussian curvature on the surface; they remove the degeneracy between the locally identical surfaces, such as the P, G and D. The concept of packing homogeneity is quantified by the construction of a skeleton-like surface-graph that is centered within the labyrinthine domains called the *Medial Surface* (MS) or *medial axis* [10–12].

The paper provides explicit geometric data for the variations in channel diameter and Gaussian curvature on a number of IPMS. We formulate a heuristic energy functional that incorporates the notion of a preferred channel diameter (induced, for example, by a preferred molecular chain length) with the conventional (local) bending energy and analyse its generic implications to relative stability of various structures. At this stage, we refrain from assigning relative weights to stretching versus bending contributions. In our view, the elucidation of geometric principles is more important than detailed quantitative analysis based on models that — owing to the intricacies of the physical system — incorporate many parameters, few of which can be measured directly. At the very least, gaining an understanding of the geometric principles is a necessary precursor to such calculations.

We note at the outset that non-local measures of relative stability are necessarily dependent on dimensions, unlike previous local energy measures — an unavoidable complication when bending and stretching energies are coupled.

2 Previous homogeneity analyses

Appreciation of the importance of surface homogeneity to self-assembly processes is not new. Anderson et al. analysed the frustration between chain stretching and film bending in cubic type II lyotropic liquid crystals: two approximately parallel surfaces (the $H = 0$ interface and the polar headgroup surface in type II systems) either have variations in the curvature and constant distance (real parallel surfaces), or constant mean curvature at the expense of variations in the thickness [14]. Another early account of the competition of bilayer thickness and curvature is given by Sadoc and Charvolin [15]. Helfrich and Hyde independently ascertained that fluctuations of the Gaussian curvature of the IPMS correspond to frustration in lyotropic systems [16,17]. Schwarz and Gompper have published similar results including distributions of the Gaussian curvature [18,19]. Their ensemble of candidate geometries, while comprising the more unusual F-RD, I-WP, S and C(P) surfaces, is restricted to cubic symmetries.

Duesing et al. give a measure for packing frustration in inverse hexagonal, micellar and the cubic bicontinuous Diamond phase. Their measure is essentially the second moment of the distribution of distances between the interface surface and the skeletal *line* graph [20]. We argue that the MS distance function is a more robustly defined and more appropriate measure. Fogden and Hyde published second moments of the distribution of Gaussian curvatures of the continuous one-parameter IPMS families analysed here [10].

A useful global variable for crystalline hyperbolic interfaces is the *homogeneity index* $\mathcal{H} = -A^{3/2}/(\sqrt{2\pi\chi}V)$, a scale-invariant parameter relating global properties V, A and integrated Gaussian curvature $2\pi\chi$ (topology) [11,17,21]. This index combines scale-invariance with independence of the choice of surface motif, n; the latter issue muddies simpler scale-invariant surface to volume ratios of the form $A/V^{2/3}$ [22]. The variable was associated with 'homogeneity' due to the observation that a fictional hyperbolic partition of constant curvature (and hence constant MS distance function or channel diameter) has the value of 3/4. However, the homogeneity index does not afford a global bound for hyperbolic interfaces: e.g. one member of Schwarz' Hexagonal surface (H) has large curvature fluctuations and nevertheless the "ideal" value of 3/4 [10], see also below. However, we retain this name for consistency, though it is a misnomer.

The homogeneity measures proposed in this article, based on variations of channel diameters, have been analysed for the cubic Primitive, Diamond and Gyroid surfaces by Schröder et al. [12]. Preliminary data for the rPD surface family has been published in [23].

3 Helfrich-like systems and homogeneity

Supramolecular aggregation, driven by total immiscibility of distinct moieties of the molecules, results in a two-dimensional surface that lies between and bounds the immiscible domains; their interior volumes can be modelled by foliations of parallel surfaces. In some cases, those domains are thickened sheets with a preferred thickness, alternatively, they may be bounded only by the cleaving surface and their interiors consist of the sub-volume to one side of the surface. In either situation, the domains' shape is determined by the local and global geometry of the cleaving surface. The notion of local surface homogeneity, with small curvature variations on the surface, pervades all theories of self-assembly that are based on Helfrich energy-functionals [24]. Both local and global homogeneity — governed by curvature and thickness variations — arise naturally in materials whose constituent molecules have a single distinct preferred shape. That shape may be determined by simple stereo-chemical requirements, as in small amphiphiles ("shape parameter" [21,25]), or indirectly result in order to maximise chain entropy in larger copolymer materials. The thickness is due to a well-defined average molecular length. The curvature of the interface is

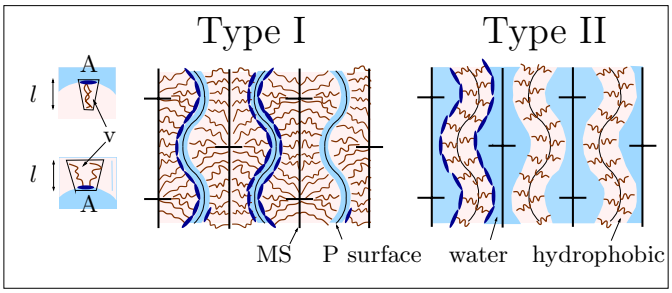

Fig. 1. Surfactant self-assembly as an example where a preferred curvature K_0 and distance function d_0 arises from the typical molecular shape: surfactant molecules may be characterised by the shape parameter $V/(A\,l)$ where A is the head group area, l the average chain length and V the volume per molecule. These amphiphilic molecules rearrange water (and possibly oil) in such a way that they pack with their tails in a hydrophobic (oily) phase and their headgroup towards the water. The shape of the molecule determines the preferred curvature. Two types of mesophases are distinguished, illustrated by a cross-section (along [110]) through the P surface. Type II where two water-channels are separated by a hydrophobic bilayer, and type I, where a layer of water separates two hydrophobic channels. These hydrophobic regions can be hydrocarbon chains with or without additional oil. The MS can be considered as the "chaotic zones" [28].

set by the variation in cross-sectional area of the molecule from end-to-end, or the molecular splay. The optimal spatial structure for such systems consists of surfaces with curvatures and space tiling properties (defined rigorously below) that match the typical molecular shape. We restrict our discussion to the special case of interfaces with vanishing mean curvature $H = 0$. This constraint simplifies the analysis, yet remains physically reasonable. It is relevant, for example, to molecular assemblies such as an amphiphilic bilayer composed of identical opposed monolayers, or symmetric multi-block copolymer assemblies. The mathematical surface describing the bilayer geometry is located in the centre of the bilayer, equidistant from the pair of surfaces describing the hydrophobic-hydrophilic interface at each monolayer. Due to the monolayer symmetry, we assume that the bilayer mid-surface has vanishing mean curvature (H).

The intricacies of systems whose interfaces are hyperbolic arise because an ideal, locally and globally homogeneous, surface does not exist in our space, leading to inherent frustration. Hyperbolic geometry tells us that a surface with constant negative Gaussian curvature cannot be smoothly embedded in three-dimensional Euclidean space [26,27].

Figure 1 illustrates the relationship between surface curvatures and tiling properties and the average molecular shape for a lipid/surfactant self-assembly process. We emphasise that this is only *one* example for a system with preferred curvature/thickness, and that the analysis of this paper is not restricted to that particular system.

We characterise the space tiling properties of a surface as follows. Introduce the distance function d: $S \to \mathbb{R}^+$ for all points on the surface S. For a point $p \in S$ the distance $d(p)$ is defined as the radius of the largest sphere that fits within one labyrinth and touches p; the sphere is centred at $p+d(p)\,N(p)$, where $N(p)$ is the surface normal at point p. This distance function measures the 'thickness' of the volume element (or the point-wise channel radius). The meaning of $d(p)$ is clear from consideration of the transport of a surface point along its normal direction, i.e. $p' = p + r\,N(p)$ with increasing positive r. For sufficiently small r, p remains the closest surface point to p'. However, as r increases beyond $d(p)$, p ceases to be the closest surface point to p', see Figure 3. In this sense, $d(p)$ measures the depth (or length) of the infinitely narrow space tile associated with the infinitesimal surface patch at point p, i.e. the local thickness of the labyrinth at point p. A further discussion of this definition is given in Section 5 and Figure 3.

With these definitions we introduce a simple energy functional

$$H(S) = \int_S \left[\alpha\,(K(p) - K_0)^2 + \beta\,(d(p) - d_0)^2\right] dS \quad (1)$$

where K_0 is the preferred Gaussian curvature and d_0 the preferred distance. α and β are positive constants. This functional has two independent elastic moduli: α and β. The former is related to the usual saddle spay modulus governing curvature energies in the Canham-Helfrich functional, as described in equation (5) below. The latter modulus is related to molecular compressibility, induced by the energetics of trans-gauche isomerism in shorter-chain molecules or chain refolding in macromolecules.

Equation (1) is insufficient to induce molecular self-assembly into defined shapes, as it neglects surface tension. We mimic this effect by constraining the total surface area to adopt a certain value (e.g. the sum of the head group sizes in lipid self-assembly). Note that equation (1) includes integrals whose contribution to the total energy scales with the total area (αK_0^2 and βd_0^2).

It is important to note that the energy functional in equation (1) penalises deviations from the preferred Gaussian curvature K_0 and preferred distance d_0 rather than from the average Gaussian curvature $\langle K\rangle$ and average distance $\langle d\rangle$. The two are in general different, $\langle K\rangle \neq K_0$ and $\langle d\rangle \neq d_0$. Deviations from the preferred (x_0) and average ($\langle x\rangle$) values of a variable x are related by the equation

$$\langle (x - x_0)^2\rangle = \langle (x - \langle x\rangle)^2\rangle + (\langle x\rangle - x_0)^2. \quad (2)$$

We introduce area averages of the relevant geometric variables, viz. $\langle x\rangle = (1/A)\int_S x\,dS$, where A denotes the surface area $A = \int_S dS$ of the cleaving surface. We deal here exclusively with crystalline surfaces and adopt the convention that S refers to an *asymmetric patch* of the surface, containing n patches in toto. The asymmetric patch is chosen with respect to the space group of the oriented surface, i.e. the group that specifies all symmetries of a single labyrinth only (excluding symmetries that exchange labyrinths). An asymmetric patch is that portion of the surface contained within an asymmetric volume of the (oriented) space group. The choice of patch is

arbitrary, however all measures are independent of that specific choice. We emphasise also that all measures analysed in this article are intensive in a thermodynamic sense, i.e. they do not depend on the size of the surface patch on which they are analysed, provided it is representative and the length scale is fixed. We are also free to choose an enlarged 'asymmetric' patch formed within an asymmetric volume of a lower-symmetry embedding of the surface (e.g. the asymmetric domain of the rhombohedral setting of the cubic G surface) without affecting the measures. The curvature measures can be deduced within a contracted asymmetric patch, associated with the asymmetric volume of the non-oriented space group of the surface (including symmetry elements that exchange the two sides of the surface). Given that the pair of labyrinths need not be symmetrically related in a generic IPMS, measures involving the distance function are better calculated with respect to the asymmetric patch of the oriented surface. That allows equation (1) to be rewritten:

$$H = n\,A\left[\alpha\langle(K-\langle K\rangle)^2\rangle + \alpha(\langle K\rangle - K_0)^2 + \beta\langle(d-\langle d\rangle)^2\rangle + \beta(\langle d\rangle - d_0)^2\right]. \quad (3)$$

Note that n is a variable, unconstrained by the system. In particular, this implies that fixing the total area ($n\,A$) alone is not sufficient to set the length scale of the system, even if only a single model geometry was considered (see also Sect. 6).

Motivated by equation (3), we define the fluctuations of Gaussian curvature, ΔK and of the distance function, Δd as the standard deviation of the respective distributions

$$\Delta K = \sqrt{\langle(K-\langle K\rangle)^2\rangle} \qquad \Delta d = \sqrt{\langle(d-\langle d\rangle)^2\rangle}. \quad (4)$$

Analyse first the local curvature contributions to the energy functional of equation (3). With the help of equation (2) this is readily transformed into a more tractable form. Introduce the asymmetric surface patch, S, with averaged Gaussian curvature $\langle K\rangle$ and area A. The Euler-Poincaré characteristic $\chi(S)$ of the asymmetric patch follows from the global Gauss-Bonnet theorem, $\int_S K dS = -2\pi\chi(S)$. Introducing the saddle splay modulus, $\overline{k}_c = 2\alpha K_0$, leads to the curvature contribution to the energy functional:

$$H_C = n\,A\left[\frac{\overline{k}_c}{2K_0}\langle K^2\rangle + 2\pi\overline{k}_c\frac{\chi}{A} + \frac{\overline{k}_c K_0}{2}\right]. \quad (5)$$

Note that the last two terms in the brackets are topological invariants and material constants respectively, independent of the length scale adopted by the surface as long as n does not change.

Consider next the contributions of the global geometry to the energy functional of equation (3) via the thickness terms. The adoption of an elastic functional about a preferred layer thickness, d_0 is a useful starting point, of varying physical relevance, depending on the molecular make-up of the assembly. Bicontinuous geometries for block copolymers are well-known [29–31]. In contrast to lyotropic systems, copolymeric molecules tile space without extra components, so that the domains occupied by the polymeric chains tessellate space. The free energy of copolymeric assemblies can be modelled in terms of entropy of self-avoiding Gaussian chains. That model induces an effective thickness for each copolymer block [32][1]. For copolymeric materials then, packing homogeneity, achieved by minimising the magnitude of Δd encodes crudely the propensity for chains to have a preferred end-to-end distance. The interpretation of distance variations (Δd) as a chain stretching contribution in molecular binary or ternary lipid (or surfactant) self-assembly is immediately relevant to bicontinuous type I lyotropic amphiphile-water mixtures, containing a pair of hydrophobic labyrinthine domains, whose hydrocarbon chain ends lie buried within the domains, see Figure 1. For these assemblies, the chain stretching energy is related to Δd if the water film separating the two labyrinths is of constant thickness.

Some energetic contribution of global geometrical features related to the domain thickness d is certain, even in cases (such as type II lipid self-assembly) where we are unable to offer an explicit model. Local contributions to the energy, based on curvature expansions, are strictly valid in the limit of vanishing bilayer thickness compared to bilayer curvature[2]. For example, the ratio of chain lengths to channel radii in lyotropic bicontinuous mesophases typically fall between 1:1 and 2:1. For example, the unit-cell length of the type II $Im\overline{3}m$ phase in DDAB-cyclohexane-water is 116 Å, with approximately 600 atoms per unit-cell and a chain length of 10–13 Å. The ratio of the minimum diameter (116/4 Å) of the P surface to the chain length is roughly 1:2 [34]. Such ratios indicate that global shape contributes to a significant degree to the relative stablity of various geometries.

4 Continuous families of IPMS

We study one-parameter families of IPMS that are symmetry degradations of the cubic Primitive, Diamond and Gyroid surfaces, retaining either three- or four-fold symmetries. Parametrisations of these surfaces are presented in [10], some additional detail and a complete list of all symmetry sites in [35], and a discussion of the channel graph structure and visualisations in [36]. The free parameters of the surfaces, r_0 or ϕ_0, arise from the Weierstrasss parametrisation formulae for minimal surfaces, that associate an embedding of the minimal surface in 3D Euclidean space with the (unit) normal vectors of the surface, via the Gauss map, whose domain is the complex plane. (The Gauss map is essentially determined by the surface normals at the 'flat points' of minimal surfaces, where the

[1] That paper incorrectly claims that the most homogeneous morphology is based on the D surface. Here we correct that assertion.

[2] Note that, given the possibility of surface transformations preserving minimality (such as rG, rPD, tP, etc.), incorporation of higher order terms is necessary even in this limit for consistency with thermodynamic stability [33].

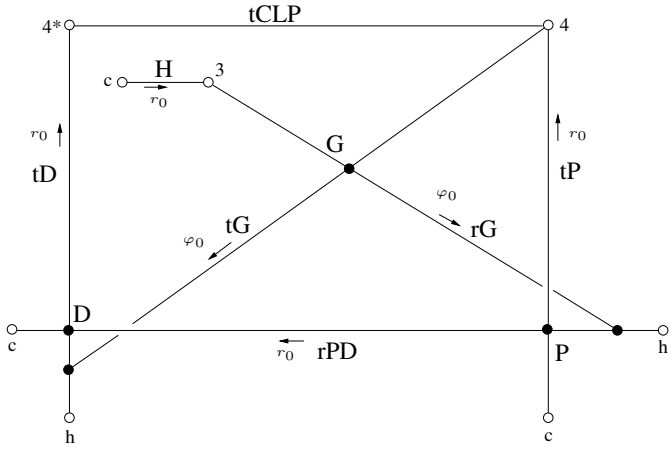

Fig. 2. Schematic layout of the three cubic IPMS and the pathways of their 3- and 4-fold generalisations and relatives. The terminals (open circles) of the families are labeled 3 and 4 representing saddle towers of this symmetry (* denotes the adjoint), or h and c to indicate helicoid and catenoid. Arrows indicates the direction in which the free parameters chosen to parametrise the surfaces increase (adapted from Fig. 3 in [10]; in that figure the order of the P, h and the rG endpoint along the line representing the rPD family, and similarly for the tD, was incorrect).

surfaces Gaussian curvature vanishes.) The flat points are located in the complex plane at $\omega_0 = r_0 \exp(i\phi_0)$. Note that the two parameters r_0 and ϕ_0 are not independent, hence resulting in one-parameter families. Figure 2 shows a schematic layout of the surface families in terms of their single complex parameters r_0 and ϕ_0. Although this exact parametrisation procedure is mathematically convoluted, and calls on some understanding of differential geometry and complex analysis, it affords significant advantages over other more approximate methods to deduce IPMS geometry. For example, the span of realisable unit cell deformations for the IPMS families emerges at once from this approach.

Generic members of the tetragonal tG IPMS family, parametrised by the value of ϕ_0, retain the 4-fold rotational symmetry of the cubic Gyroid, but not the 3-fold symmetry [10]. For $\phi_0 = -\pi/4$, the tG surface coincides with the cubic Gyroid; $\phi_0 = 0$ corresponds to a member of the tD surface family. For $\phi_0 = -\pi/2$ it becomes the 4-fold "saddle tower" [37] where the lattice period a goes to infinity. The tD and tP surface families [38] retain the 4-fold symmetry of the cubic D and P surfaces, respectively. They are adjoints of each other with free parameter r_0. In the limit $r_0 \to 0$ the tP approaches the catenoid; for $r_0 \to 1$ the tP surface approaches the one-periodic 4-fold saddle tower. The cubic P surface is realised for $r_0 = (2-\sqrt{3})^{1/2} \approx 0.51764$. Similarly, the tD surface approaches the one-periodic helicoid as $r_0 \to 0$ and the adjoint of the 4-fold saddle tower at $r_0 \to 1$. For $r_0 = (2-\sqrt{3})^{1/2} \approx 0.51764$ corresponds to the cubic D surface. For $\phi_0 = 0$, the endpoint of the tG family is realised with $r_0 = 0.43188$.

The rhombohedral (rG) IPMS examples retain the three-fold rotational symmetries and lose four-fold symmetries of the cubic Gyroid; members of the one-parameter family are parametrised by ϕ_0 [39,11]. The rG surfaces with $\phi_0 = 0$ also belongs to the rPD surface family; the rG surface with $\phi_0 = -\pi/6$ is the so-called HG or Lidinoid surface [40]; $\phi_0 = -\pi/3$ gives the cubic Gyroid and as $\phi_0 \to -\pi/2$ the rG surfaces approach the three-fold saddle tower [37]. Rhombohedral distortions of the P and D surfaces yield, somehow surprisingly, a single surface family rPD with free parameter r_0. When $r_0 = 0.49472$, the rPD surface is coincident with the $\phi_0 = 0$ endpoint of the rG surface; $r_0 = 1/\sqrt{2}$ gives the cubic P, $r_0 = \sqrt{2}$ the cubic D. As $r_0 \to 0$ the surfaces apporach the helicoid, for $r \to \infty$ they approach the catenoid.

Finally, Schwarz' Hexagonal (H) surfaces are a one-parameter family of IPMS, with free parameter r_0. Unlike the other IPMS families that exhibit isolated higher symmetry members, the symmetry of all members of the H family remains unchanged on deformation; the member with $r_0 = 0.49701$ corresponds to the maximum stretch $c/a = 0.8840$ (in both symmetry settings that include and exclude the inversion symmetry of the surface, viz. $P\overline{6}m2$ and $P6_3/mmc$ respectively). As $r_0 \to 1$, the H surfaces approach the three-fold saddle-tower, found also as an endpoint of the rG surface family.

These complex symmetry and surface relations between IPMS families allow a number of pathways between the P, D, and Gyroid cubic surfaces, such that all intermediate structures are themselves IPMS without self-intersections. In particular, there are two paths connecting the cubic D and G, one of rhombohedral symmetry (D→ rPD → P → D → rPD → rG → G) and one of tetragonal symmetry (D → tD → tG → G).

The ensemble of these surface families includes, apart from the tCLP surface, all IPMS of the regular class [41,42] that represent pathways between the cubic P, D and G surfaces. Here we restrict ourselves to the above mentioned IPMS families. Note, however, that if one relaxes the requirement that the transition structures are minimal surfaces, other pathways can be found. In particular, some nodal surfaces (implicit surface parametrisations as level-sets of sums over Fourier modes [43–45]) provide pathways between IPMS, via intermediates that are close to IPMS.

5 Medial surfaces and space partitions

The medial surface (MS) represents a bounded domain in three-dimensional Euclidean space $\mathbb{E}^3$ as a surface skeleton centered within that domain [10,11]. Unlike simpler transforms, such as skeletal graphs, the MS retains all information about the topology *and* geometry of the domain, when combined with an additional scalar quantity, the *distance function* mentioned above [46].

We apply the usual definition of the MS to the case of a periodic domain C in three-dimensional Euclidean space $\mathbb{E}^3$ that is bounded by an IPMS S [12]. The domain C is the subset of $\mathbb{E}^3$ on one of the two sides of S. We assume that the normal field N on S is normalised, i.e. $|N(p)| = 1$

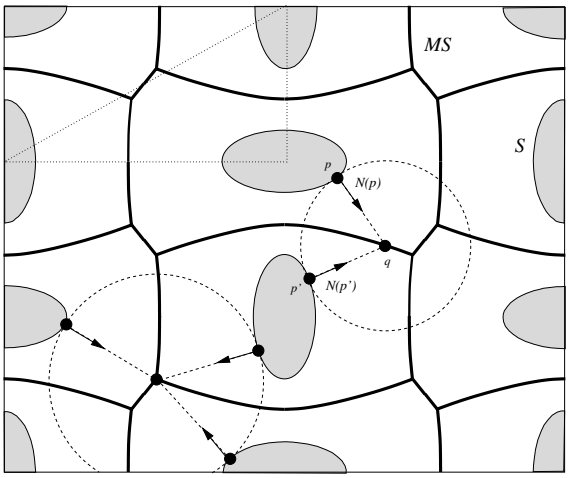

Fig. 3. 2D illustration of the medial surface construction for a domain C (white) which is the complement of a symmetric set of ellipses. The two dashed circles are maximal disks, with centres on the MS. Also shown is the asymmetric unit of the structure (dotted triangle) from which the entire structure is obtained by application of symmetry operations.

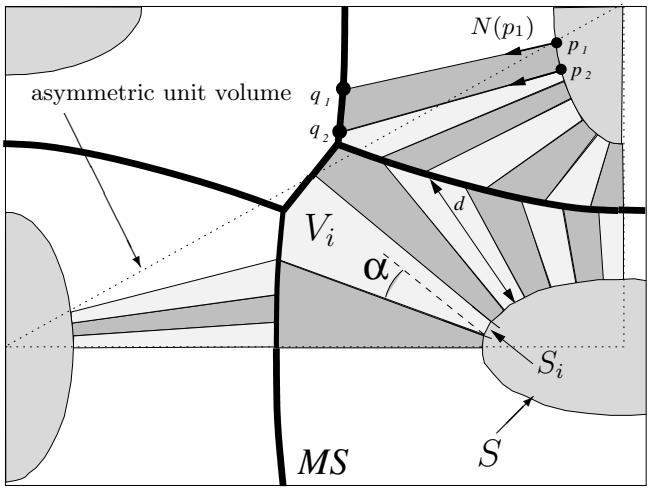

Fig. 4. Illustration of the space partition used to define homogeneity. The cells corresponding to the asymmetric unit are alternately colored in light and dark gray. The angle α is indicative of the local curvature K.

for all $p \in \mathcal{S}$, and that it points into C. The differentiability of $\mathcal{S}$ implies that N is smooth.

The MS of domain C is the locus of centers of all *maximal spheres* in C, defined to be spheres which are fully contained in C and not fully contained in any other sphere in C. These maximal spheres touch S in two or more points, as well as limit points of the domain. It follows from this definition that every point p on S is mapped uniquely onto a corresponding point $q = ms(p)$ on the MS. Namely, the touching points of the maximal spheres are mapped onto their centres. Therefore, the medial surface transform is given by the equation

$$ms : S \to C, \qquad p \mapsto ms(p) := p + d(p)\, N(p), \qquad (6)$$

where N is the normal field of S and d: $S \to \mathbb{R}^+$ is called the distance or radius function. Note that the reverse map is not unique. Figure 3 illustrates the MS construction.

An algorithm to compute the MS of IPMS, based on earlier work by Amenta et al. [47,48] and others [49–53], has been described in [12]. Its input is a triangulated surface (such as in [35]) sampling an asymmetric unit patch of the IPMS, together with surface normals at each triangular surface facet. The algorithm is Voronoi-based; it computes the 3D Voronoi diagram of the sample points on S. Then, for each sample point p it assigns the intersection of the ray $p + [0, \infty]\, N(p)$ with the Voronoi cell $V_c(p)$ of point p as the MS point $ms(p)$.

The MS construction yields a partition of space into prismatic volume elements that are thin but long, extending normal to the IPMS. This space partition is particularly suited for analyses of local (intrinsic) and global (extrinsic) homogeneity. Figure 4 illustrates the construction for the 2D case: the surface $S = \partial C$ (or its asymmetric patch if symmetries are present) is subdivided into small area elements S_i. A volume element V_i, associated with each S_i, is defined as the space between S_i and its image $ms(S_i)$ on the MS. We assume that the area elements are so small that the variations of the MS distance function d and of the Gaussian curvature K over the points of an individual S_i are negligible. Then the volume elements are characterised by the surface area A_i of S_i, the length $d = \langle d(p) \rangle = \int_{S_i} d(p)/A_i$ and the volume v_i of V_i. Note that the volume, V_i, associated with a surface patch, S_i, comprises only one of the two IPMS subvolumes. Throughout this article, V denotes the volume on *one* side of the IPMS only.

For computational purposes we use the facets of the triangulation of S as area elements. The volume elements are simple polytopes bounded by the triangle $\{p_1, p_2, p_3\}$ on S, its image $\{q_1, q_2, q_3\}$ where $q_i = ms(p_i)$ and the fourgons $\{p_i, p_j, q_j, q_i\}$ with $\{i, j\} = \{1, 2\}, \{2, 3\}, \{3, 1\}$. The average distance function is computed over the three vertices, $d = \sum_{i=1}^{3} d(p_i)/3$.

The MS construction is sensitive to small changes of the surface normal field N. In particular, the volume tiles V_i are finitely long, with their length given by $d(p)$, even if the area tiles S_i are infinitesimally small; see the appendix of [12] for further discussion. This sensitivity is common to all surface measures that depend on the surface normal. For example, both the Gaussian and mean curvature are sensitive to such variations; these curvatures are of direct physical relevance to many systems, via the Helfrich functional.

A detailed description of the MS geometry of the cubic P, D and G surfaces is given in [12], and of the surface families discussed here in [36].

6 Length scale normalisation

IPMS are by their nature scale-free, i.e. rescaling of the coordinates $\{x', y', z'\} = \{\Gamma x, \Gamma y, \Gamma z\}$ for any finite factor Γ does not affect their vanishing mean curvature. However, the distance function, the Gaussian curvature and

higher moments of their distributions, are sensitive to the length-scale. Hence, comparison of these parameters for different surfaces is dependent on the length scale chosen for each surface. Here we focus on purely geometric concepts (hence avoiding the formulation of an energy functional that fully determines the length scale). Accordingly, we analyse all surfaces for three distinct length-scale normalisations: (i) the average distance function $\langle d \rangle$; (ii) the surface-to-volume ratio V/A; or (iii) the average Gaussian curvature $\langle K \rangle$ are constant.

For any finite positive factor Γ and any surface S the rescaling operation

$$\{x', y', z'\} = \{\Gamma x, \Gamma y, \Gamma z\} \tag{7}$$

defines an affinely transformed surface S'. The Gaussian curvature, the surface-to-volume ratio, the surface area and the MS distance function of S' are given by

$$K' = \frac{1}{\Gamma^2} K, \quad \frac{V'}{A'} = \Gamma \frac{V}{A}, \quad A' = \Gamma^2 A, \quad d' = \Gamma d. \tag{8}$$

The same scaling holds for their averages $\langle K' \rangle$ and the standard deviation $\Delta K' = \sqrt{\langle K'^2 \rangle - \langle K' \rangle^2}$ (and similarly for V'/A' and d'). The following scaling factors lead to surfaces with normalised $\langle K \rangle$, $\langle d \rangle$ or V/A:

$$\Gamma = \sqrt{\langle -K \rangle} \quad \Leftrightarrow \quad \langle K' \rangle = \frac{1}{\Gamma^2} \langle K \rangle = -1 \tag{9}$$

$$\Gamma = 1/(V/A) \quad \Leftrightarrow \quad \frac{V'}{A'} = \Gamma \frac{V}{A} = 1 \tag{10}$$

$$\Gamma = 1/\langle d \rangle \quad \Leftrightarrow \quad \langle d' \rangle = \Gamma \langle d \rangle = 1. \tag{11}$$

Note that the normalisation to constant $\langle K \rangle$ also implies, by virtue of the global Gauss-Bonnet theorem, that the surface area per integrated curvature A/χ is constant. Within each individual surface family (where χ is constant) that implies that A is constant. However, normalisation to constant A for all surfaces is *not* well-defined, since the choice of surface unit (S) is arbitrary. Indeed, for any surface S, A can be adjusted to any integer multiple ($n\,A$), either by taking n copies of the patch without changing the length scale, or by adjusting the length scale according to equation (8) with $\Gamma = \sqrt{n}$. In other words, for the total interface, the area A can be normalised for arbitrary scaling by adjusting the number of translational unit cells or asymmetric unit patches. We refer also to the discussion in the appendix of [54].

7 Homogeneity of rPD, rG, H, tD, tP and tG

This section presents data for extrinsic and intrinsic homogeneity (in the sense of Sect. 3) as well as for the average Gaussian curvature and distance function values for the tG, tP, tD, rG, rPD and H surface families. These data are presented for the three distinct length-scale normalisations introduced in the previous section. In the following we use the term *global (local) homogeneity* for the value of Δd (ΔK), with optimal homogeneity corresponding to a minimum of that quantity.

Figures 5 and 6 give data for ΔK, Δd, $\langle K \rangle$ and $\langle d \rangle$ for all six surface families and various length scale normalisations. In addition, Figures 8 and 9 provide V/A and symmetry group parameters, useful for structure identification from symmetry data. Table 1 lists numerical values of all relevant parameters for extrema and other relevant surface members.

All numerical data for $\langle d \rangle$ and Δd is computed for triangulated patches of the asymmetric surface patches and MS points from the MS algorithm described in Section 5. The asymmetric patches (of the space groups of the oriented surfaces) were sampled with similar density of approximately 2500 points for the H, rPD, tD and tP surface, corresponding to 5000 points for tG and rG. In addition, some of the rPD members were sampled at approximately twice that density in the vicinity of the cubic P. All curvature, surface area, volume and lattice parameter data stems from analytic expressions derived from the Weierstrass parametrisation containing elliptic integrals [11,35]. These were evaluated using standard numeric integration.

A first observation is that the behaviour of the homogeneity measures is qualitatively similar for all three length scale normalisations considered, at least in the properly three-periodic regime (sufficiently far from the aperiodic or 1- or 2-periodic limits). In particular, the minima of ΔK, Δd, $\langle d \rangle$ and $\langle K \rangle$ occur, within the resolution of our data, at the same values of the free parameters, independent of the normalisation[3].

The local (curvature) homogeneity data confirms previous results: the most symmetric embeddings (i.e. cubic) of the rPD, tG, rG, tD, tP generic families display optimal local homogeneity. For all normalisations the (cubic) D, P and G surfaces are local minima of ΔK, relative to rhombohedral and tetragonal distortions that retain the minimal surface feature. For normalised $\langle K \rangle$, their absolute values ($\Delta K/\langle K \rangle^2$) are equal, due to the (Bonnet) isometry between these surfaces [10]. In contrast, surface scaling to give normalised $\langle d \rangle$ or V/A lifts this degeneracy, leaving the G as the most locally homogeneous, followed by the D and then the P. We note that the sequence P $\rightarrow$ D $\rightarrow$ G, observed in previous analyses [19], is due to this effect.

Our analysis reveals that packing homogeneity, quantified by Δd, is locally minimal for the cubic D and G surfaces with respect to rhombohedral (rPD, rG) and tetragonal (tG, tD) IPMS deformations, regardless of normalisation. Therefore, these two cubic IPMS minimise distance fluctuations as well as curvature variations with respect to rhombohedral or tetragonal relatives. Hence, *both* global *and* local homogeneity can be simultaneously optimised by formation of these two cubic surfaces.

[3] Note that for the minimum of Δd of the H surface, this statement is only correct within the resolution of our data. A slight shift of the extremum is unavoidable: the unnormalised function $\Delta d(r_0)$ has a minimum at r_{min}. The normalising functions $\Gamma_1(r_0) = A/V$ and $\Gamma_2(r_0) = sqrt\langle -K \rangle$ are strictly monotonic decreasing at r_{min} and not identical. Hence, the minima of $\Delta d(r_0) \times \Gamma_1$ and $\Delta d(r_0) \times \Gamma_2$ cannot be at exactly the same value.

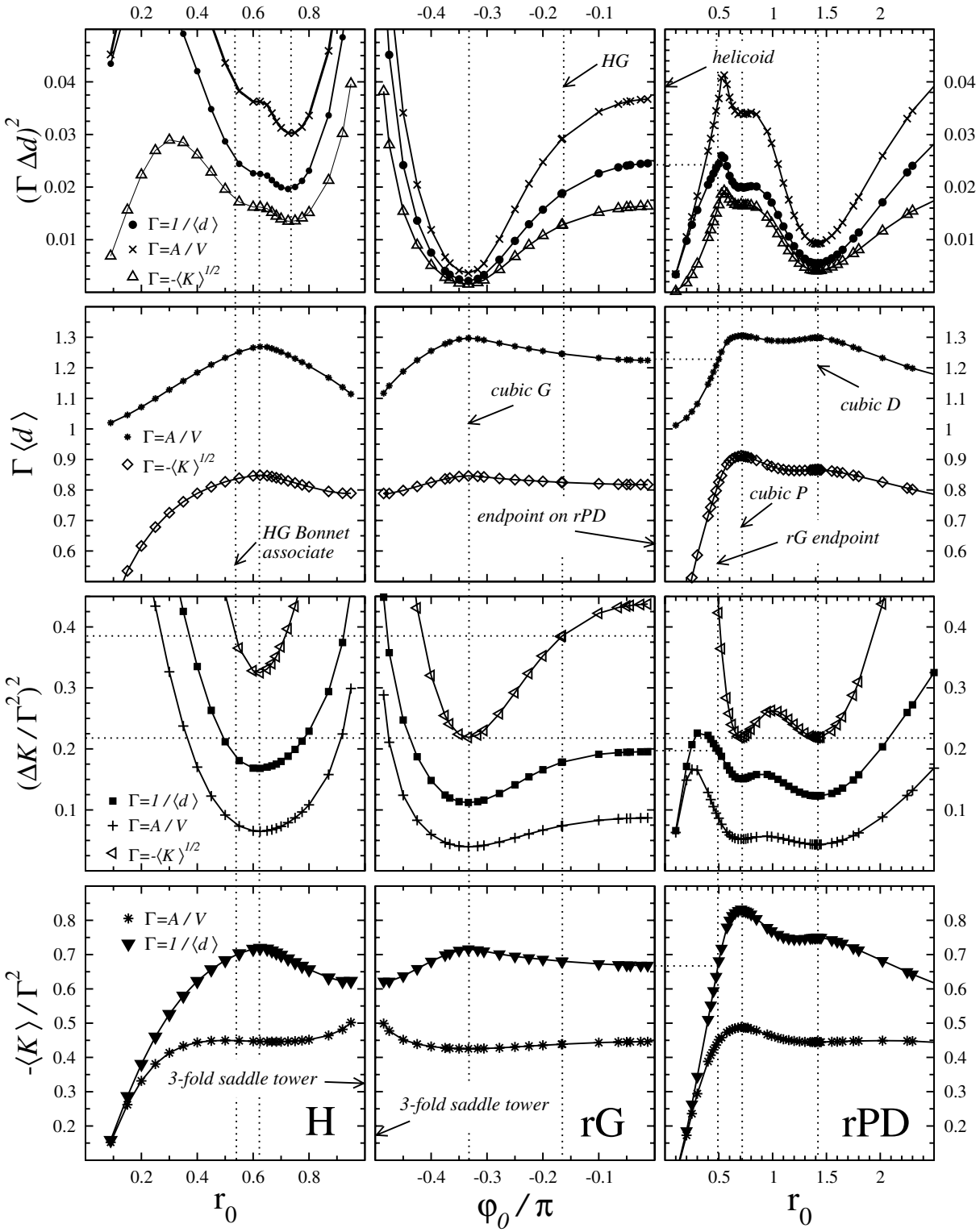

Fig. 5. Homogeneity of H (left column), rG (middle) and rPD (right) surface families. The x-axes represent the free parameter of the respective surface family. The first row are the fluctuations Δd of the channel width (as measured by the MS distance function), the second row the average channel width, the third row the fluctuations ΔK of the Gaussian curvature and the fourth row the average $\langle -K \rangle$ of the Gaussian curvature. The different symbols within each plot represent the three possible length scale normalisations to constant V/A, $\langle d \rangle$ and $\langle K \rangle$ (Each normalisation corresponds to the prefactors Γ given in equations (9–11). Within each column (row), the x-axes (y-axes) have the same scale. Note that the volume V is the volume on one side of the surface, i.e. of one of the two labyrinths only.

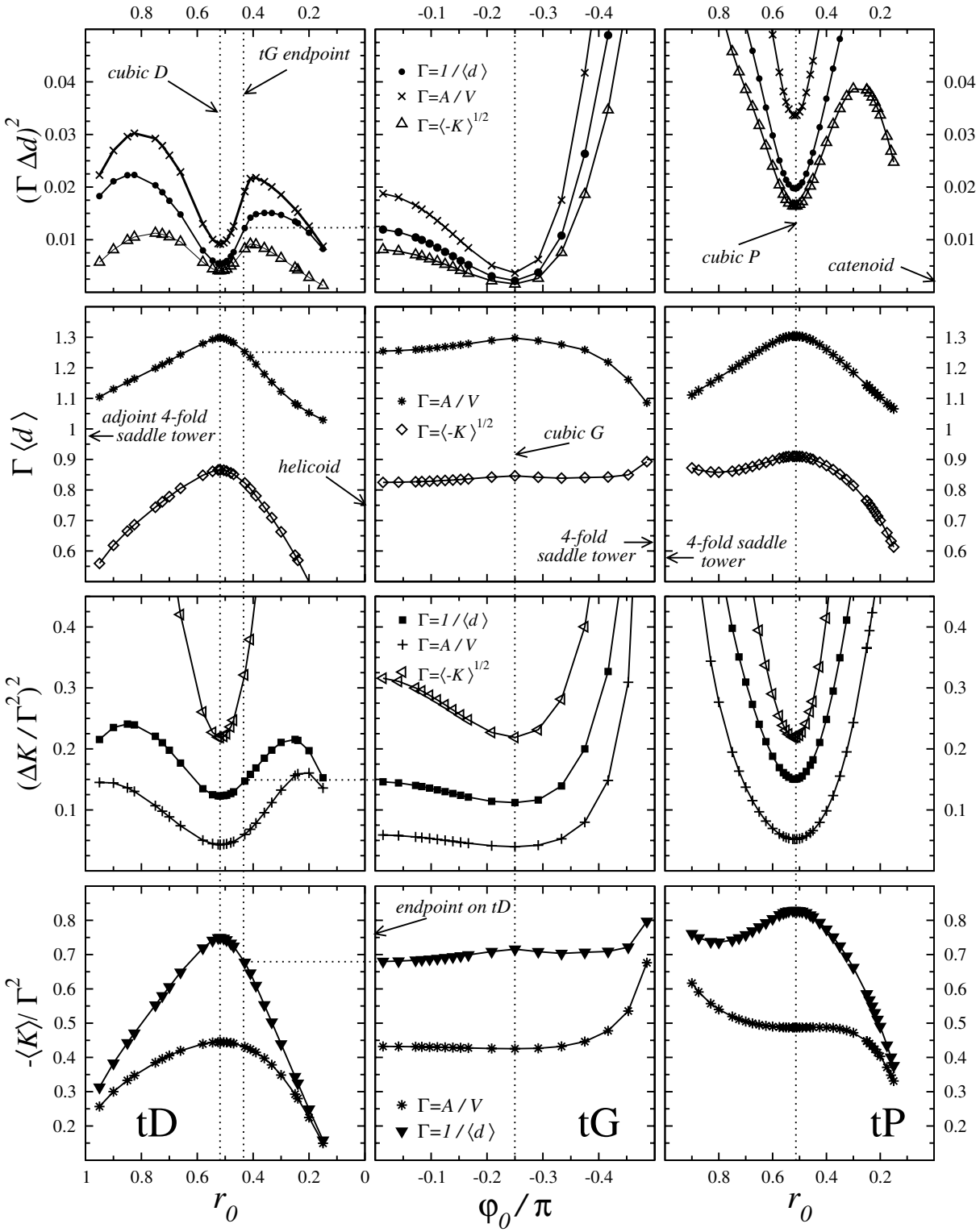

Fig. 6. Homogeneity of tD (left column), tG (middle) and tP (right) surface families. See the caption of Figure 5 for details.

Table 1. Values of the various properties at significant points of the surface families. The space groups given are for the oriented surfaces. χ is the Euler-Poincaré characteristic of the asymmetric unitpatch in those spacegroups, and A its surface area. a and c are the lattice parameters. See Figures 5 to 9 for the full functional dependence of these properties on the free parameter of the TPMS family. Note that the volume V is the volume on one side of the surface, i.e. of one of the two labyrinths only.

			$V/A = \text{const.} = 1$, $r = A/V$						
	significance	$\mathcal{H}$	$r^2(\Delta d)^2$	$r\langle d\rangle$	$\frac{(\Delta K)^2}{r^4}$	$\frac{\langle K\rangle}{r^2}$	$r\,a$	$r^2\,A$	c/a
r_0	**Hexagonal H**, $P\overline{6}m2$, $\chi = 1/3$								
0.40534	$\mathcal{H} = 3/4$	0.7500	0.0581	1.1874	0.1642	0.4444	5.3192	4.7123	0.8677
1/2	max. c/a	0.7458	0.0436	1.2330	0.0916	0.4495	5.2666	4.6595	0.8840
0.53607	adj. of HG	0.7462	0.0395	1.247	0.0774	0.4490	5.2737	4.6645	0.8813
0.62059	min. curv. fluc.	0.7481	0.0362	1.2687	0.0648	0.4467	5.3281	4.6890	0.8591
0.735	min. dist. fluc.	0.7480	0.0302	1.2373	0.0820	0.4469	5.4603	4.6868	0.7978
ϕ_0	**rG**, $R32$, $\chi = 2/3$								
$-\pi/3$	cubic G	0.7667	0.0037	1.2974	0.0396	0.4253	8.7439	9.8483	0.6124
$-\pi/6$	HG	0.7550	0.0291	1.2459	0.0739	0.4385	8.0426	9.5519	0.7633
r_0	**rPD**, $R\overline{3}m$, $\chi = 1/3$								
0.49472	rG endpoint	0.7488	0.0368	1.2241	0.0870	0.4458	7.8825	4.6978	0.7975
0.53	max. dist. fluct.	0.7372	0.0412	1.2559	0.0750	0.4600	7.5957	4.5530	0.8638
$1/\sqrt{2}$	cubic P	0.7163	0.0335	1.3046	0.0519	0.4872	6.6329	4.2989	1.2247
1	max of $\Delta K/\langle K\rangle^2$	0.7355	0.0277	1.2876	0.0562	0.4622	5.8715	4.5316	1.8612
$\sqrt{2}$	cubic D	0.7498	0.0092	1.2983	0.0432	0.4446	5.4274	4.7104	2.4495
2.02134	max c/a	0.7461	0.0260	1.2309	0.0883	0.4491	5.2700	4.6630	2.6488
r_0	**tD**, $I4_1/amd$, $\chi = 1/4$								
0.43188	rG $\phi_0 = 0$	0.7607	0.0188	1.2546	0.0591	0.4320	5.9028	3.6360	1.1315
0.51764	cubic D	see rPD with $r_0 = \sqrt{2}$					5.4275	3.5329	1.4142
ϕ_0	**tG** , $I4_122$, $\chi = 1/2$								
0	endpoint on tD	see tD with $r_0 = 0.43188$					5.9028	7.2720	1.1315
$-\pi/4$	cubic G	see rG with $\phi_0 = -\pi/3$					6.1831	7.3870	1
r_0	**tP** , $P4/mmm$, $\chi = 1/4$								
0.51764	cubic P	see rPD with $r_0 = \sqrt{2}$					4.6902	3.2242	1

In contrast, frustration between local and global homogeneity constraints arise for the P family. Although the cubic P surface minimises local curvature inhomogeneities, as well as distance fluctuations within the tP family, it is not a minimum, but an inflection point of Δd, along the rPD family. Indeed, the P surface can be transformed into the D surface via rPD surfaces such that all intermediate members are more packing homogeneous than the P. That observation holds within the precision of our data, ± 0.01 in $(\Delta d)^2$.

Local and global homogeneity measures for Schwarz' H(exagonal) IPMS family also exhibit distinct behaviours. The values of the free parameter for H surface members that optimise local and global homogeneity measures are not the same. Figure 7 shows a close-up of the quantities $\Gamma^2\Delta K$ and $\Delta d/\Gamma$ normalised to constant V/A, i.e. $\Gamma = A/V$. The minimum of $\Gamma^2\Delta K$ is at $r_0 = 0.62059$, whereas the minimum of $\Delta d/\Gamma$ is at $r_0 = 0.735$ for all normalisations Γ of equations (9–11). This discrepancy leads to a frustration in a system with energy functional given by equation (1). The dimensionless and intensive

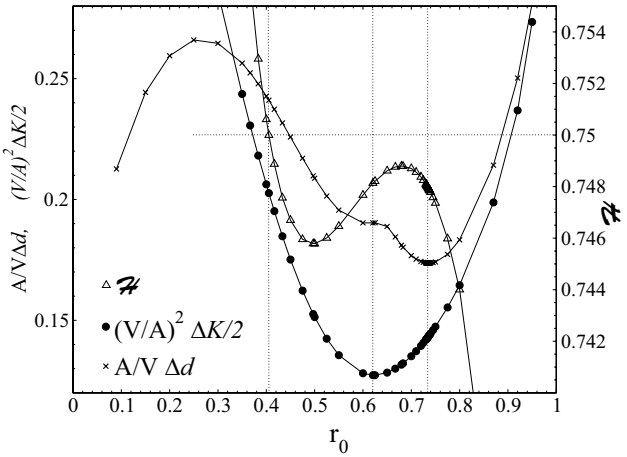

Fig. 7. Homogeneity data for Schwarz' hexagonal surface (H). The values of the free parameter A for which the fluctuations of the curvature and the fluctuations of distance function are minimal and for which $\mathcal{H} = 3/4$, are different. The behaviour for normalisations to constant $\langle d\rangle$ and $\langle K\rangle$ is qualitatively similar, and omitted for the sake of clarity.

Table 2. Continuation of Table 1.

	$\langle K\rangle$ = const. = 1, $r=\sqrt{\langle -K\rangle}$						$\langle d\rangle$ = const. = 1, $r=1/\langle d\rangle$					
r	$r^2(\Delta d)^2$	$r\langle d\rangle$	$\frac{(\Delta K)^2}{r^4}$	$r\,V/A$	$r\,a$	$r^2\,A$	$r^2(\Delta d)^2$	$\frac{(\Delta K)^2}{r^4}$	$\frac{\langle K\rangle}{r^2}$	$r\,V/A$	$r\,a$	$r^2\,A$
r_0	**Hexagonal H**											
0.40534	0.0258	0.7916	0.8314	0.6667	3.5461	2.0944	0.0412	0.3264	0.6266	0.8422	4.4798	3.3425
1/2	0.0196	0.8267	0.6862	0.4535	3.5309	2.0944	0.0287	0.2118	0.6834	0.8110	4.2713	3.0648
0.53607	0.0177	0.8358	see HG	0.6701	3.5338	see HG	0.0254	0.1874	0.6985	0.8018	4.2282	2.9984
0.62059	0.0162	0.8479	0.3249	0.6683	3.5609	2.0944	0.0225	0.1680	0.7190	0.7882	4.1995	2.9129
0.735	0.0135	0.8271	0.4107	0.6685	3.6501	2.0944	0.0197	0.1922	0.6841	0.8082	4.4131	3.0615
ϕ_0	**rG**											
$-\pi/3$	0.0016	0.8461	0.2188	0.6522	5.7026	4.1888	0.0022	0.1121	0.7159	0.7708	6.7395	5.8507
$-\pi/6$	0.0127	0.8250	0.3841	0.6622	5.3259	4.1888	0.0187	0.1780	0.6807	0.8026	6.4553	6.1537
r_0	**rPD**											
0.49472	0.0164	0.8174	0.4376	0.6677	5.2631	2.0944	0.0246	0.1953	0.6681	0.8169	6.4392	3.1350
0.53	0.0190	0.8518	0.3542	0.6782	5.1517	2.0944	0.0261	0.1865	0.7256	0.7962	6.0478	2.8864
$1/\sqrt{2}$	0.0163	0.9106	0.2188	0.6980	4.6297	2.0944	0.0197	0.1504	0.8292	0.7665	5.0842	2.5258
1	0.0128	0.8754	0.2629	0.6798	3.9917	2.0944	0.0167	0.1544	0.7663	0.7766	4.5600	2.7332
$\sqrt{2}$	0.0041	0.8657	0.2188	0.6668	3.6191	2.0944	0.0054	0.1229	0.7495	0.7702	4.1803	2.7944
2.02134	0.0117	0.8249	0.4376	0.6702	3.5318	2.0944	0.0171	0.2027	0.6805	0.8124	4.2813	3.0776
r_0	**tD**											
0.43188	0.0081	0.8246	0.3165	0.6573	3.8797	1.5708	0.0120	0.1463	0.6800	0.7971	4.7050	2.3101
0.51764	see rPD with $r_0=\sqrt{2}$				3.6190	1.5708	see rPD with $r_0=\sqrt{2}$				4.1804	2.0959
ϕ_0	**tG**											
0	see tD with $r_0=0.43188$				3.8797	3.1416	see tD with $r_0=0.43188$				4.7050	4.6202
$-\pi/4$	see rG with $\phi_0=-\pi/3$				4.0323	3.1417	see rG with $\phi_0=-\pi/3$				4.7662	4.3894
r_0	**tP**											
0.51764	see rPD with $r_0=\sqrt{2}$				3.2737	1.5708	see rPD with $r_0=\sqrt{2}$				3.5951	1.8943

homogeneity index $\mathcal{H} = A^{3/2}/(\sqrt{-2\pi\chi}V)$ [11,21,17] for the H surface family is also shown in Figure 7. The H surface has a member, $r_0 = 0.40534$, for which it adopts the value 3/4 (once believed to indicate optimal homogeneity). It has already been shown that that value does not correspond to minimal curvature fluctuations [10]; neither does it minimise global packing inhomogeneities, see also Figure 5 and Table 1.

It is interesting to compare homogeneity data for the cubic P IPMS with the most locally homogeneous member of the H surface family, $r_0 = 0.62059$. To our surprise, we find that this H surface is almost as homogeneous as the cubic P surface, in terms of both local and global measures.

Consider next the energy cost due to curvature and distance fluctuations for the various pathways between the surfaces, displayed in Figure 2. In particular, there are two paths connecting the cubic D and G: one of rhombohedral symmetry (D→ rPD → P → rG → G) and one of tetragonal symmetry (D → tD → tG → G). Among these paths, the tetragonal one is far more homogeneous than the rhombohedral. In terms of both global and local homogeneity, the intersection point of tD and tG is the most inhomogeneous point along the tetragonal path, with curvature fluctuations ΔK^2_{max} and Δd^2_{max}. For the rhombohedral path, the most locally inhomogeneous point is the rG endpoint on the rPD (at $r_0 = 0.49472$), whereas the most globally inhomogeneous point is on the rPD at $r_0 = 0.53$. For the rhombohedral path, relative to the homogeneity of the G given by ΔK^2_G and Δd^2_G, the local homogeneity barrier $(\Delta K^2_{max} - \Delta K_G)^2)/\Delta K^2_G$ is 1.20 (0.73, 1.0) and the global homogeneity barrier $(\Delta d^2_{max} - \Delta d_G)^2)/\Delta d^2_G$ is 9.8 (10.8, 10.9), for constant V/A ($\langle d\rangle$, $\langle K\rangle$). For the tetragonal path the local barrier is 0.49 (0.3, 0.45) and the global 3.9 (2.7, 6.5), again for constant V/A ($\langle d\rangle$, $\langle K\rangle$). As a reference, $\Delta K^2_D/\Delta K^2_G = 0.091$ (0.096, 0) and $\Delta d^2_D/\Delta d_G = 0.60$ (1.45, 0), and $\Delta K^2_P/\Delta K^2_G = 0.2$ (0.3, 0) and $\Delta d^2_P/\Delta d_G = 2.6$ (2.6, 0)

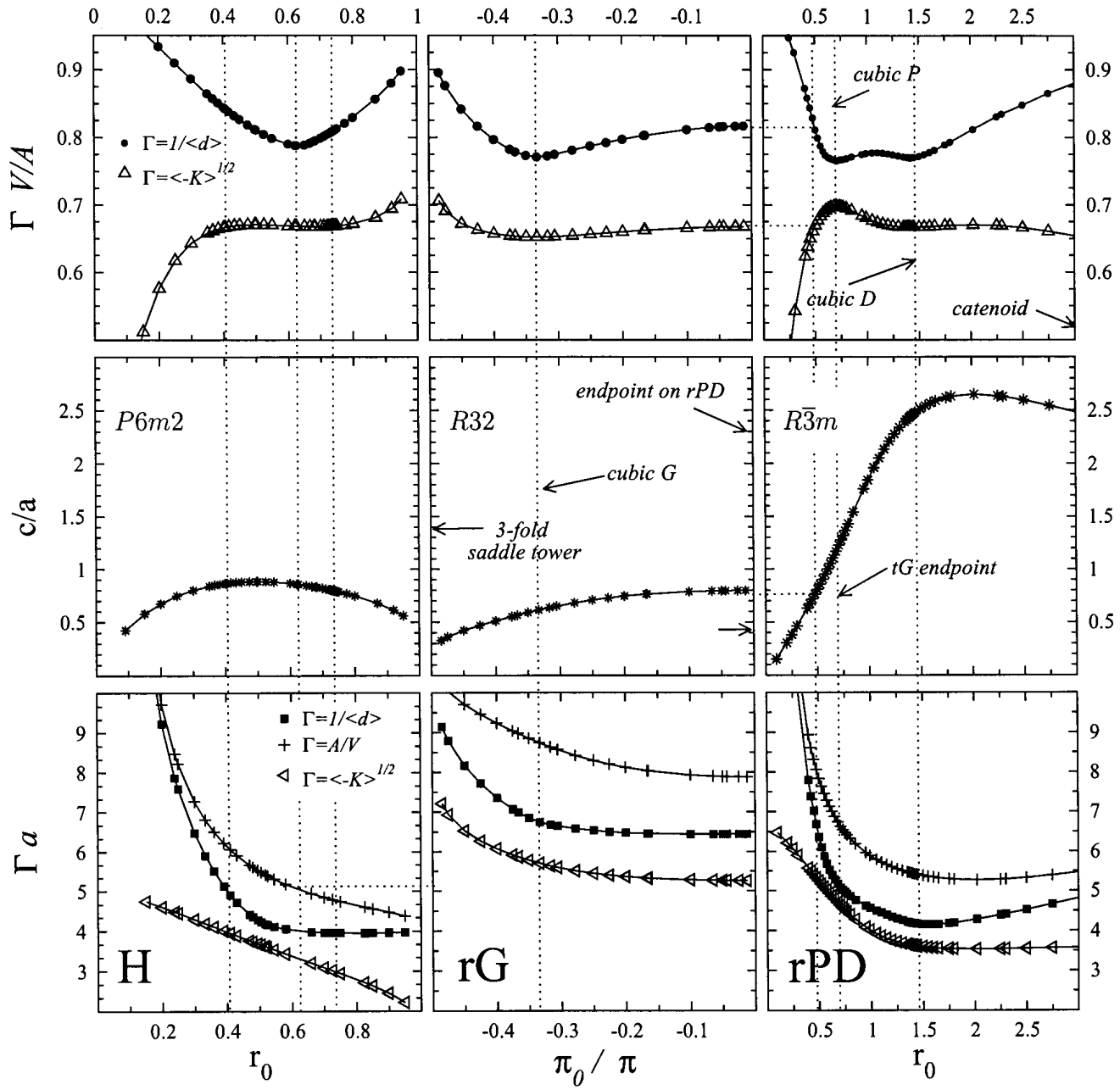

Fig. 8. Normalised volume-to-surface ratio V/A, lattice parameter ratio c/a and normalised lattice parameter a as a function of the free parameter for the H, rG and rPD surface families. Within each column (row), the x-axes (y-axes) have the same scale. Note that the volume V is the volume on one side of the surface, i.e. of one of the two labyrinths only.

for constant V/A ($\langle d \rangle$, $\langle K \rangle$). Hence, the tetragonal path incurs approximately half the energy cost of the rhombohedral path.

A transition from the optimal H member to the cubic Gyroid via the H family and the rG family is relatively unfavourable, due to large penalties in both curvature and distance functions: the large values of Δd and ΔK at the three-fold saddle tower (the $r_0 = 1$ member of the H and the $\phi_0 = -\pi/2$ of the rG) make that route unlikely. (This result too holds for all three length scale normalisations.)

Thus far, we have only considered the fluctuations of K and d around their average values. A precise assessment of the implications of deviations of the average quantities, $\langle K \rangle$ and $\langle d \rangle$, from the preferred values, K_0 and d_0, is not possible without assigning relative weights for curvature and packing contributions in equation (1). However, we note that for constant V/A the expression $\Gamma\, d = d\, A/V$ is reminiscent of the "shape parameter" used to predict lipid self-assembly geometries [25]. For the analysis of phase transitions between D and G (both of which are assumed to be stable phases and with very similar values for $d\, A/V$), a path with small variations of that quantity should be favourable. Again, the tetragonal path has smaller variations than the rhombohedral path.

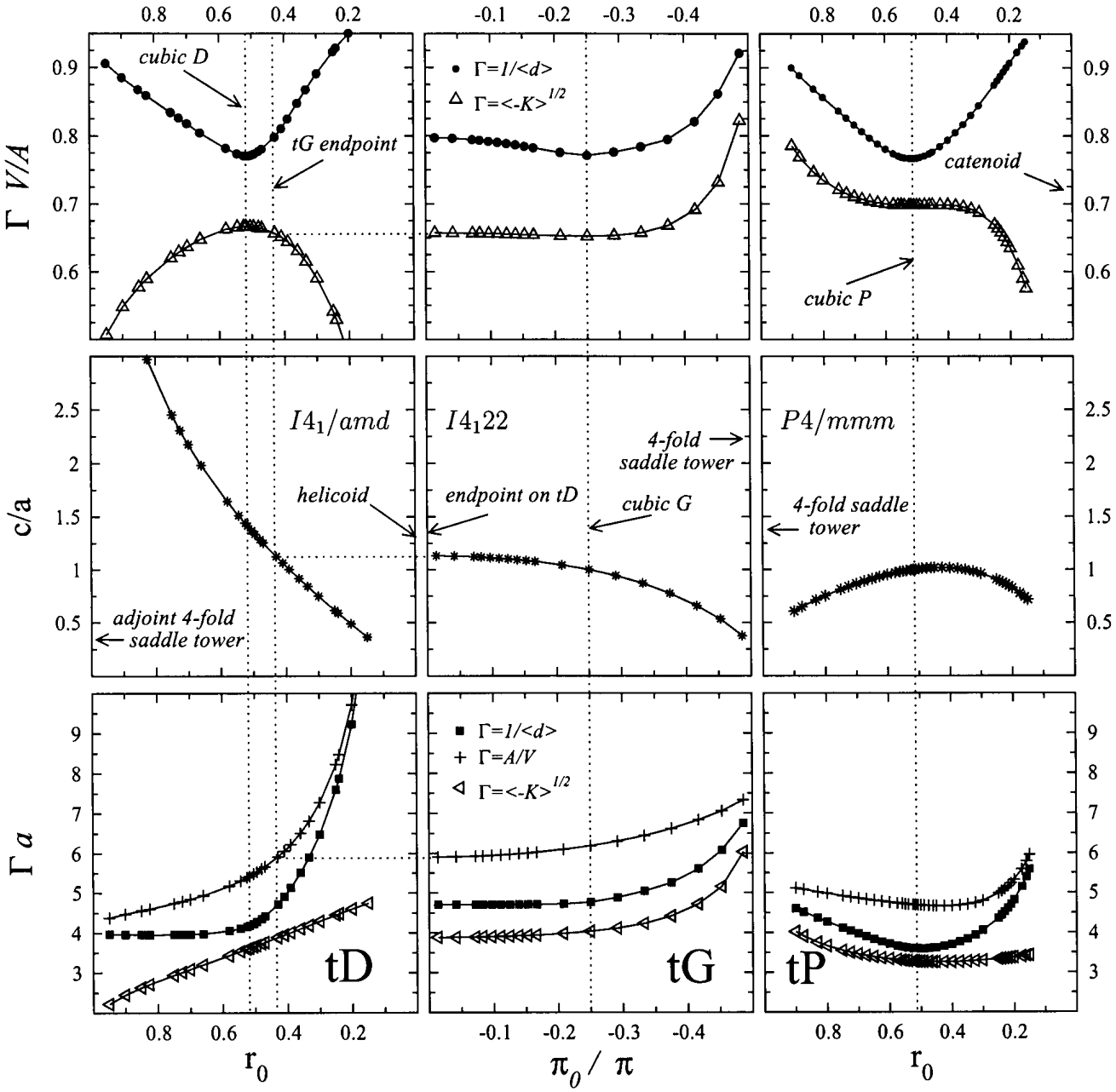

Fig. 9. Normalised volume-to-surface ratio V/A, lattice parameter ratio c/a and normalised lattice parameter a as a function of the free parameter for the tD, tP and tG surface families. Within each column (row), the x-axes (y-axes) have the same scale. Note that the volume V is the volume on one side of the surface, i.e. of one of the two labyrinths only.

So far, we have omitted any discussion of the minimal surfaces that emerge as end-points of these surfaces families. Those limit cases are no longer 3-periodic as some lattice vectors diverge, leaving zero- and one-periodic minimal surfaces. The zero-periodic case is the the catenoid, one-periodic surfaces are the 3- and 4-fold *saddle towers* and the helicoid. Consider the behaviour of ΔK, $\langle K\rangle$, Δd and $\langle d\rangle$ for the 3- and 4-fold saddle towers (rG and tG with $\phi_0 = -\pi/2$). The fluctuations ΔK and Δd are large, in fact $\Delta d \to \infty$. (The behaviour of all quantities involving the Gaussian curvature is a subtle one in that limit, as $\langle -K\rangle/(A/V)^2 \to \infty$, see [35] for details. Our diagrams do not indicate that behaviour as the plot range is too limited.) Viewed from a distance, these surfaces consist of 3 and 4 asymptotically flat sheets, smoothly connected along a common 3- or 4-fold axis. In the vicinity of that axis, the surfaces form one-periodic strings of channels, oriented along distinct directions, of finite radius r_h. The distribution of distance function values then ranges from r_h to ∞.

In contrast to all other minimal surfaces, the catenoid – that emerges as the $r_0 \to \infty$ member of the rPD and $r_0 = 0$ of the tP family – is not a balanced surface, i.e. its two sides are different. The fluctuations of Δd and ΔK for the

catenoid are larger than for periodic examples. For these three limiting surfaces, global and local inhomogeneities are larger than related measures for 3-periodic IPMS.

The 1-periodic helicoid (the $r_0 = 0$ member of the rPD and tD) requires more subtle reasoning concerning its homogeneity, as ΔK and Δd assume very small values. This is a consequence of the periodic sheet structure which is, apart from its rotational screw axis, reminiscent of a stacking of asymptotically flat lamellae (the translational lattice vector is now perpendicular to the sheets). This causes very small variations of the distance function (as between two parallel planes). Indeed, the helicoid is a very homogeneous space partition, but for a planar geometry rather than a labyrinth geometry. This is evidenced by the average curvature $\langle K \rangle = 0$ and distance function value (or shape parameter) $\Gamma \langle d \rangle = \langle d \rangle A/V = 1$. This example is one where deviations of average measures from their preferred values dominate the point-wise deviations around the average.

8 Conclusion

Our analysis of the packing and curvature homogeneities of the tG, tP, tD, rPD, rG and H IPMS families and their zero-, one- and two-periodic end-members allows some generic conclusions to be drawn regarding (i) the relative stabilities of various minimal surface geometries as molecular assemblies and (ii) the relative feasibilities of continuous IPMS pathways between homogeneous three-periodic IPMS. This work, together with [10], demonstrates unequivocally that the cubic Diamond and Gyroid surfaces are distinct local maxima of the homogeneity, both in terms of curvature and packing homogeneity. This result holds regardless of the normalisation chosen (to either constant V/A, constant average Gaussian curvature or constant average distance function). For these two surfaces, there is no competition between curvature and packing homogeneity. This result goes some way towards explaining why the cubic Gyroid and Diamond IPMS are so commonly found in liquid-crystalline self-assemblies.

Among the three cubic geometries, the Gyroid is the most homogeneous: for constant V/A and $\langle d \rangle$, it has minimal curvature fluctuations, and for constant $\langle K \rangle$ the curvature fluctuations are, due to the Bonnet isometry, identical for P, D and G. The distance function fluctuations are also minimal for the Gyroid, followed by the D and the P geometries (see also [12]). That conclusion may explain the prevalence of G mesophases in block copolymeric systems, whose free energies favour local and global homogeneity. It is commensurate with our analysis that the only reported bicontinuous type I lipid mesophase (i.e. the MS distance function can be identified with the hydro-carbon chain length) is Q230 with cubic Gyroid symmetry $Ia\bar{3}d$, reported by Luzzati et al. [55].

A further key result is that the cubic P surface is not an optimum of the global (distance) homogeneity, despite its locally optimal local (curvature) homogeneity. Within the precision of our calculations, the P surface represents an inflection point of the fluctuations of the distance function d; all deformations along the rPD towards the D surface have lower fluctuations of d than the P. In particular, this means that a stable phase with geometry of the cubic P surface is globally frustrated. Therefore molecular-assemblies whose energy is strongly dependent on domain thicknesses (e.g. those with strongly preferred chain lengths and curvatures comparable to the chain length) are far less likely to adopt the P surface geometry than the D or G. We note that the P mesophase has been detected in soft mixed-molecular assemblies, including surfactant-water mixtures and polymer-lipid-water mixtures [56]; to our knowledge it has not been reported in pure copolymer systems, although it has been found in copolymer-ceramics nanocomposites [57]. It is noteworthy that the presence of the P surface geometry in liquid crystals comprised of a single chemical species (and hence subject to homogeneity constraints) has been the subject of much debate over the past few years. For example, the early report of a P mesophase in the SDS-water system [58] has not been reproduced since and the mesostructure of the thermotropic $Im\bar{3}m$ mesophase has remained elusive, apparently fitting neither the P surface nor the I-WP surface (another $Im\bar{3}m$ IPMS) geometry [59].

Our analysis of Schwarz' H surface was motivated by the observation that one member (at $r_0 = 0.41$) has the 'optimal' value of 3/4 for the scale-invariant homogeneity index $\mathcal{H}$, yet large curvature fluctuations [10]. We find that in addition to high curvature fluctuations at that member (more than double compared to the minimum at $r_0 = 0.62$) it also has high distance function fluctuations (approximately 1.5 times the minimum value at $r_0 = 0.735$). However, the H surface has members with fluctuations Δd of the distance function that are slightly lower than those for the cubic P surface, for all three normalisations; the curvature fluctuations ΔK at those members are only slightly higher than those of the P. These data suggest that the H surface is as likely to be found in molecular assemblies as the P. We note that the c/a axial ratio of any H surface does not exceed $c/a = 0.8840$ (both in the space group $P\bar{6}m2$ of the oriented and $P6_3/mmc$ of the non-oriented surface) — approximately half the value of hexagonal closed-packed spheres ($c/a = 1.6330$ [60]. It is therefore unlikely that the mesostructures of hexagonal mesophases in mesoporous silicates [61] and amphiphilic molecules — whose axial ratios are similar to those of close-packed spheres — are related to H surfaces [62].

We have also shown that the lowest energy pathway linking the optimal bicontinuous geometries, the G and D structures, is a continuum of embedded, three-periodic IPMS of tetragonal symmetries ($I4_1acd$ and $I4_1/amd$), related to the cubic G and D IPMS, viz. the tG and tD surfaces (see [11,36] for illustrations of these surface families). It is clear that this low-energy continuum of embedded and minimal surfaces (the only one with tetragonal symmetry) provides a seemingly favourable transition path between the G and D cubic geometries. We speculate that it may also open the possibility of stable hybrid geometries between the G and D surfaces. Thus, experimentalists should

not overlook the possibility of non-cubic 'intermediate' bicontinuous mesophases of tetragonal symmetries.

Lastly, these data support a long-standing speculation in the self-assembly literature. The very existence of isotropic, three-periodic crystalline mesophases in soft materials, whose energy is governed by preferred (hyperbolic) curvature and domain thicknesses, is a result of the relative homogeneity of crystalline geometries relative to other forms, including two-periodic and less symmetric structures.

S.T.H. acknowledges the Australian Research Council for financial support through a Federation Fellowship.

References

1. M. Pisani, S. Bernstorff, C. Ferrero, P. Mariani, J. Phys. Chem. B **105**, 3109 (2001)
2. L. Saturni, F. Rustichelli, G. Di Gregorio, L. Cordone, P. Mariani, Phys. Rev. E **64**, 040202 (2001)
3. A. Squires, R. Templer, O. Ces, A. Gabke, J. Woenckhaus, J. Seddon, R. Winter, Langmuir **16**, 3578 (2000)
4. A. Squires, R. Templer, J. Seddon, A. Gabke, J. Woenckhaus, R. Winter, T. Narayanan, S. Finet, Phys. Rev. E **72**, 011502 (2005)
5. R.H. Templer, J.M. Seddon, N.A. Warrender, A. Syrykh, Z. Huang, R. Winter, J. Erbes, J. Phys. Chem. **102**, 7251 (1998)
6. L. Ellison, D. Michel, F. Barmes, D. Cleaver, Phys. Rev. Lett. **97**, 297801 (2006)
7. T.F. Bailey, M. Cordell, T. Epps, F. Bates, Macromolecules **35**, 7007 (2002)
8. T.H. Epps, E.W. Cochran, T.S. Bailey, R.S. Waletzko, C.M. Hardy, F. Bates, Macromolecules **37**, 8325 (2004)
9. G. Schröder, Ph.D. thesis, Australian National University, Canberra, Australia (2005)
10. H. Blum, J. Theor. Biol. **38**, 205 (1973)
11. L.R. Nackman, Computer Graphics and Image Processing **20**, 43 (1982)
12. G.E. Schröder, S.J. Ramsden, A.E. Christy, S.T. Hyde, Eur. Phys. J. B **35**, 551 (2003)
13. A. Fogden, S. Hyde, Eur. Phys. J. B **7**, 91 (1999)
14. D.M. Anderson, S.M. Gruner, S. Leibler, Proc. Natl. Acad. Sci. USA **85**, 5364 (1988)
15. J. Sadoc, J. Charvolin, J. Phys. France **48**, 1559 (1987)
16. W. Helfrich, H. Rennschuh, *Landau Theory of the Lamellar-to-Cubic Phase Transition*, in *Colloque de Physique C7-1990* (1990), Supplément au J. Phys. France, pp. 189–195
17. S. Hyde, *Curvature and the global structure of interfaces in surfactant-water systems*, in *Colloque de Physique C7-1990* (1990), Supplément au Journal de Physique, pp. 209–228
18. U. Schwarz, G. Gompper, Phys. Rev. E **59**(5), 5528 (1999)
19. U. Schwarz, G. Gompper, Phys. Rev. Lett. **85**(7), 1472 (2000)
20. P. Duesing, R. Templer, J. Seddon, Langmuir **13**, 351 (1997)
21. S. Hyde, S. Andersson, K. Larsson, Z. Blum, T. Landh, S. Lidin, B. Ninham, *The Language of Shape*, 1st edn. (Elsevier Science B. V., Amsterdam, 1997)
22. A. Schoen, Tech. rep., NASA (1970)
23. G. Schröder, S. Ramsden, A. Fogden, S. Hyde, Physica A **339**, 137 (2004)
24. W. Helfrich, Z. Naturforsch. **28c**, 693 (1973)
25. J.N. Israelachvili, D.J. Mitchell, B.W. Ninham, J. Chem. Soc. Faraday Trans. 2 **72**, 1525 (1976)
26. D. Hilbert, Transactions of the A.M.S. 2 pp. 87–99 (1901)
27. M. Spivak, *Comprehensive Introduction to Differential Geometry*, Vol. 3 (Wilmington, DE, Publish or Perish Press, 1979)
28. V. Luzzati, R. Vargas, P. Mariani, A. Gulik, H. Delacroix, J. Mol. Biol. **229**, 540 (1993)
29. H. Hasegawa, H. Tanaka, T. Hashimoto, C. Han, Macromolecules **20**, 2120 (1987)
30. H. Hasegawa, H. Tanaka, K. Yamasaki, T. Hashimoto, Macromolecules **20**, 1651 (1987)
31. E. Thomas, D. Anderson, C. Henkee, D. Hoffman, Nature **334**, 598 (1988)
32. A. Fogden, S. Hyde, G. Lundberg, J. Chem. Soc. Faraday Trans **87** (7), 949 (1991)
33. R. Bruinsma, J. Phys. II France **2**, 425 (1992)
34. P. Barois, S. Hyde, B. Ninham, T. Dowling, Langmuir **6**, 1136 (1990)
35. G. Schröder-Turk, A. Fogden, S. Hyde, in preparation (2007)
36. G. Schröder-Turk, A. Sheppard, S. Hyde, in preperation (2007)
37. H. Karcher, Manuscripta Math. **62**, 83 (1988)
38. H. Schwarz, *Gesammelte Mathematische Abhandlungen. 2 Bände.* (Springer, Berlin, 1890)
39. A. Fogden, M. Haeberlein, S. Lidin, J. Phys. I France **3**, 2371 (1993)
40. S. Lidin, S. Larsson, J. Chem. Soc. Faraday Trans. **86** (5), 769 (1990)
41. A. Fogden, S. Hyde, Acta Cryst. **A48**, 442 (1992)
42. A. Fogden, S. Hyde, Acta Cryst. **A48**, 575 (1992)
43. H. Von Schnering, R. Nesper, Angew. Chem. Int. Ed. Engl. **26**, 1059 (1987)
44. H. Von Schnering, R. Nesper, Z. Phys. B – Condensed Matter **83**, 407 (1991)
45. M. Wohlgemuth, N. Yufa, J. Hoffman, E. Thomas, Macromolecules **34**, 6083 (2001)
46. E. Sherbrooke, N.M. Patrikalakis, F.E. Wolter, Graphical Models and Image Processing **58**(6), 574 (1996)
47. N. Amenta, S. Choi, R. Kolluri, Computational Geometry: Theory and Applications **19**(2-3), 127 (2001)
48. N. Amenta, S. Choi, G. Rote, *Incremental Constructions con BRIO*, in *SoCG'03, June 8–10, 2003, San Diego, California, USA* (2003), pp. 211–219
49. D. Attali, A. Montanvert, Computer Vision and Image Understanding **67**(3), 261 (1997)
50. J. Boissonnat, F. Cazals, *Natural coordinates of points on a surface*, in *Proceedings of the 16th Annual ACM Symposium on Computational Geometry* (2000), pp. 223–232
51. T.K. Dey, W. Zhao, *Approximate medial axis as a voronoi subcomplex*, in *Proceedings of the seventh ACM symposium on Solid modeling and applications* (ACM Press, 2002), pp. 356–366, ISBN 1-58113-506-8
52. J. Goldak, X. Yu, A. Knight, L. Dong, Int. J. Computational Geometry and its Applications **1**, 327 (1991)

53. D. Sheehy, C. Armstrong, D. Robinson, IEEE Transactions on Visualization and Computer Graphics **2**(1), 61 (1996)
54. K. Grosse-Braukmann, J. Colloid and Interface Science **187**, 418 (1997)
55. V. Luzzati, A. Tardieu, T. Gulik-Krzywicki, E. Rivas, F. Reiss-Husson, Nature (London) **220**, 485 (1968)
56. K. Larsson, F. Tiberg, Current Opinion in Colloid and Interface Science **9**, 365 (2005)
57. A. Finnefrock, R. Ulrich, G. Toomes, S. Gruner, U. Wiesner, J. Am. Chem. Soc. **125**, 13084 (2003)
58. P. Kekicheff, B. Cabane, J. Phys. France **48**(9), 1571 (1987)
59. A. Levelut, M. Clerc, Liquid Crystals **24**(1), 105 (1998)
60. M. O'Keeffe, B. Hyde, *Crystal Structures, I. Patterns and Symmetry* (Mineralogical Society of America Washington, USA, 1996)
61. S. Tolbert, T. Schaffer, J. Feng, P. Hansma, G. Stucky, Chemistry of Materials **9**(9), 1962 (1997), `http://dx.doi.org/10.1021/cm960454o`
62. M. Clerc, J. Phys. II France **6**, 961 (1996)